Pergamon

Int. J. Heat Mass Transfer. Vol. 40, No. 16, pp. 3899–3907, 1997

Printed in Great Britain
0017–9310/97 $17.00+0.00

PII: S0017–9310(97)00037–9

Thermal instability during the melting process in an isothermally heated horizontal cylinder

JAE DONG CHUNG and JOON SIK LEE†
Department of Mechanical Engineering, Seoul National University, Seoul 151-742, Korea

and

HOSEON YOO
Department of Mechanical Engineering, Soong Sil University, Seoul 156-743, Korea

(*Received* 30 *August* 1996 *and in final form* 20 *December* 1996)

Abstract—The present study extends the range of the Rayleigh numbers to systematically investigate the flow transition during the melting process in an isothermally heated horizontal cylinder, emphasizing the complicated multi-cell flow pattern and the thermal instability. The enthalpy–porosity formulation is employed with appropriate source terms to account for the phase-change. At the low Rayleigh number, the flow is in a stable state because a single-cell base flow is developed at the initial melting stage. At the high Rayleigh number, the Benard-type convection is found to develop within a narrow liquid gap between the unmelted solid surface and the cylinder bottom wall. At the intermediate Rayleigh number, the on-set of the Benard convection depends on the strength of the base flow under development and a delicate interaction between the two flows determines the flow pattern afterwards. The effective Rayleigh number and the corresponding wave number are in excellent agreement with those from the linear stability theory.

1. INTRODUCTION

The melting process of a phase-change material fixed in an isothermally heated horizontal cylinder is a well-known problem which has been investigated numerically and experimentally for many years. This problem has been a subject of continuous interest because controversial results have been reported. Saitoh and Hirose [1] reported experimental results which show convexed solid–liquid interface at the bottom of the unmelted solid as melting progresses. While Rieger *et al.*, [2], Ho and Viskanta [3], and Yoo and Ro [4] showed concaved interface numerically and experimentally. In view of the fact that the interface shape is directly related to flow and heat transfer during the melting process, a close examination of the source of these contradictory results is of importance in order to clearly understand the melting characteristics. In this context, Ro and Kim's recent work [5] which ascertained the existence of multi-solution made meaningful progress. They successfully showed, by the numerical analysis, that both interface shapes are possible, however, they could not explain the origin of such contradictory results.

A review of the previous studies reveals two common aspects: (1) the Rayleigh numbers considered are in the limited range; and (2) they depended only on the boundary tracking moving coordinate system or similar type of the coordinate transformation method. The former aspect is due to the fact that most of the previous studies focused on the melting process associated with the latent heat storage, and the latter is that it is easy to handle the transient moving phase-interface using such coordinate systems. However, considering that the dominant heat transfer mode is convection during the melting process, it is necessary to extend the Rayleigh number range in order to systematically investigate the transient phenomena accompanied by melting. Such a demand is substantiated because the study of the natural convection in a concentric annulus [6] claimed that flow disturbances are generated by the hydrodynamic instability for small Prandtl number fluid, while by the thermal instability for large Prandtl number fluid. Since the previous studies have been conducted for the relatively small Rayleigh numbers even though their fluid Prandtl number is large ($Pr \sim 50$), flow disturbances cannot be observed at the initial melting stage where thermal buoyancy is much weaker than viscous force. In other words, since two-cell or three-cell flow structure does not appear until the liquid gap between the solid bottom and the cylinder wall is widened enough as melting progresses, the origin of the contradictory phase-interface shapes cannot be explained in connection with flow pattern in the liquid phase near the bottom wall of the cylinder. Thus, one of the objectives of the present study is to analyze the

† Author to whom correspondence should be addressed.

NOMENCLATURE

a	critical wave number
C	specific heat at constant pressure
d	critical liquid gap
f_L	liquid fraction
f_S	solid fraction
g	gravitational acceleration
h	sensible enthalpy, $h = C_L(T - T_m)$
h_{sf}	latent heat of fusion
h_ξ, h_η	geometric factor, $h_\xi = (x_\xi^2 + y_\xi^2)^{1/2}$, $h_\eta = (x_\eta^2 + y_\eta^2)^{1/2}$
J	Jacobian
k	thermal conductivity
p	pressure
Pr	Prandtl number, ν/α_L
R_w	cylinder radius
Ra	Rayleigh number, $g\beta(T_w - T_m)R_w^3/(\nu\alpha_L)$
Ra_{eff}	effective Rayleigh number, $Ra(d/R_w)^3$
S	source term
Sc	subcooling number, $C_S(T_m - T_0)/h_{sf}$
Ste	Stefan number, $C_L(T_w - T_m)/h_{sf}$
t	time
T_0	initial temperature
T_m	melting temperature
T_w	wall temperature
u, v	Cartesian velocity components
u_ξ, u_η	covariant velocity components
U, V	contravariant velocity components
x, y	Cartesian coordinates.

Greek symbols

α	thermal diffusivity
α_ξ, α_η	geoemetric factors, $\alpha_\xi = h_\xi h_\eta^2/J$, $\alpha_\eta = h_\eta h_\xi^2/J$
β_ξ, β_η	geometric factors, $\beta_\xi = \lambda h_\eta/J$, $\beta_\eta = \lambda h_\xi/J$
Γ	exchange coefficient
λ	geometric factor, $\lambda = x_\xi x_\eta + y_\xi y_\eta$
μ	viscosity
ν	kinematic viscosity
ξ, η	transformed coordinates
ρ	density
τ	dimensionless time, $\tau = t^+ Ste$
ϕ	general dependent variable.

Superscript

$^+$	dimensionless variable
*	solid-to-liquid property ratio.

Subscript

L	liquid
nb	neighboring grid points
p	grid point
S	solid
w	cylinder wall.

high Rayleigh number flow because no report for the high Rayleigh number has been found even though the thermal instability at the initial melting stage depends strongly on the Rayleigh number. In addition, in view of the solution method, the boundary tracking moving coordinate system may be involved with uncertainty according to grid generation when the phase-interface shape is highly irregular due to multi-cell flow pattern near the bottom wall.

This study aims to reassess the melting process in a horizontal cylinder emphasizing the fact that melting characteristics such as the phase-interface shape under natural-convection-dominant condition is essentially determined by the initial flow pattern and transient progress. Particularly focused are the multi-cell flow structure and the thermal instability at the initial melting stage for the high Rayleigh number flow which has not been attempted before. The enthalpy method is employed where the phase-interface is implicitly determined in the calculation domain.

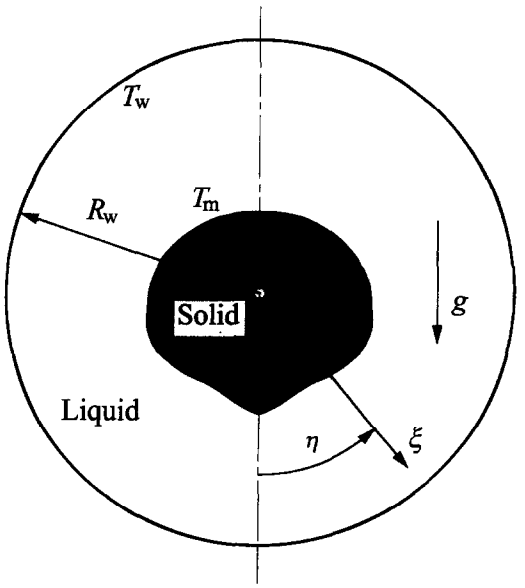

Fig. 1. Schematic diagram of the inward melting process in a horizontal cylinder.

2. ANALYSIS

As depicted in Fig. 1, the problem considered is the melting process of a phase-change material at an initial temperature of T_0 in a horizontal cylinder whose wall temperature is T_w above the melting temperature T_m. The *n*-octadecane is chosen as the test phase-change material, which is commonly used in the pre-

Table 1. Thermophysical properties of *n*-octadecane ($C_{18}H_{38}$)

Properties	Value
Melting temperature	28.18°C
Density	814 kg m^{-3}
Thermal expansion coefficient	9.1×10^{-4} K^{-1}
Viscosity	3.878×10^{-3} kg m^{-1} s^{-1}
Latent heat	2.4136×10^{5} J kg^{-1}
Specific heat of solid	1.9×10^{3} J kg^{-1} K^{-1}
Specific heat of liquid	2.2×10^{3} J kg^{-1} K^{-1}
Thermal conductivity of solid	0.390 W m^{-1} K^{-1}
Thermal conductivity of liquid	0.157 W m^{-1} K^{-1}

vious studies. The thermophysical properties are listed in Table 1. The convective flow is assumed incompressible, laminar and the Boussinesq type as usually assumed in the previous studies. The property variation between phases is neglected.

2.1. *Governing equations*

Though the governing equations in the polar coordinate system can simply be used with the enthalpy method for the present geometric configuration, the equations in the non-orthogonal coordinate system is used for the general purpose. The balance equations in the general form can be written in the two-dimensional rectangular coordinate system as follows:

$$\frac{\partial}{\partial t}(\rho\phi)+\frac{\partial}{\partial x}\left(\rho u\phi-\Gamma\frac{\partial\phi}{\partial x}\right)+\frac{\partial}{\partial y}\left(\rho v\phi-\Gamma\frac{\partial\phi}{\partial y}\right)=S(x,y). \quad (1)$$

The specific expressions for ϕ, Γ and S corresponding to mass, momentum and energy equations are listed in Table 2 in dimensionless forms. The variables are non-dimensionalized as follows:

$$x^+=\frac{x}{R_w},\quad y^+=\frac{y}{R_w},\quad t^+=\frac{\alpha_L t}{R_w^2}$$

$$u^+=\frac{uR_w}{\alpha_L},\quad v^+=\frac{vR_w}{\alpha_L},\quad p^+=\frac{pR_w^2}{\rho_L\alpha_L^2},$$

$$h^+=\frac{h}{C_L(T_w-T_m)}. \quad (2)$$

Here, the characteristics of the enthalpy method can be easily recognized, which is applicable to both solid and liquid phases. That is, by introducing an arbitrarily large number, A, to the momentum equation, it turns out to be the Navier–Stokes equation if the liquid fraction (mass fraction and volume fraction are the same because it is assumed that $\rho_S=\rho_L$), f_L, is unity, and the velocity components are forced to be zero if the liquid fraction is zero. In the energy equation, the latent heat is reflected in the source term as a function of f_L. Note that the dependent variable in the energy equation is the sensible enthalpy. Hereafter, superscript $^+$ will be omitted for convenience.

Table 2. Variables in the dimensionless governing equations

ϕ^+	Γ^+	S^+
1	0	0
u^+	$Pr\mu^*$	$-\frac{\partial p^+}{\partial x^+}-A\frac{(1-f_L)^2}{f_L^3}u^+$
v^+	$Pr\mu^*$	$-\frac{\partial p^+}{\partial y^+}+Ra\cdot Pr\cdot h^+-A\frac{(1-f_L)^2}{f_L^3}v^+$
h^+	k^*	$\frac{C_L-C_S}{C_L}\frac{\partial}{\partial t^+}(\rho^* f_S h^+)+\frac{1}{Ste}\frac{\partial}{\partial t^+}(\rho^* f_S)$

Equation (1), in the dimensionless form, can be written in a non-orthogonal coordinate system (see Fig. 1 for notation) through the transformation given by

$$x=x(\xi,\eta), y=y(\xi,\eta). \quad (3)$$

The transformed equation can be written as

$$\frac{\partial}{\partial t}(J\phi)+\frac{\partial}{\partial\xi}\left(U\phi-\frac{\alpha_\xi\Gamma}{h_\xi}\frac{\partial\phi}{\partial\xi}\right)+\frac{\partial}{\partial\eta}\left(V\phi-\frac{\alpha_\eta\Gamma}{h_\eta}\frac{\partial\phi}{\partial\eta}\right)$$
$$=JS(\xi,\eta)-\frac{\partial}{\partial\xi}\left(\frac{\beta_\xi\Gamma}{h_\eta}\frac{\partial\phi}{\partial\eta}\right)-\frac{\partial}{\partial\eta}\left(\frac{\beta_\eta\Gamma}{h_\xi}\frac{\partial\phi}{\partial\xi}\right) \quad (4)$$

where

$$U=\alpha_\xi u_\xi-\beta_\xi u_\eta,\quad V=\alpha_\eta u_\eta-\beta_\eta u_\xi \quad (5)$$

$$u_\xi=(x_\xi u+y_\xi v)/h_\xi,\quad u_\eta=x_\eta(u+y_\eta v)/h_\eta. \quad (6)$$

The computation has been conducted on the right-half of the cylinder because of the symmetry. Considering a half-circle with an infinitesimally small radius at the center of the cylinder, the lower and upper symmetry lines with respect to the center of the half-circle corresponds to $\eta=0$ and 1, respectively, and the circumference of the half-circle and the cylinder wall correspond to $\xi=0$ and 1, respectively. Thus, the boundary conditions described in the transformed coordinates are:

$$\frac{\partial U}{\partial n}=0,\quad V=0,\quad \frac{\partial h}{\partial n}=0 \quad \text{at } \eta=0 \text{ and } 1 \quad (7)$$

$$U=V=0,\quad h=1 \quad \text{at } \xi=1 \quad (8)$$

$$U=V=0,\quad \frac{\partial h}{\partial n}=0 \quad \text{at } \xi=0. \quad (9)$$

2.2. *Numerical method*

The governing equation (4) is discretized using the finite volume method and the SIMPLER algorithm is used for the pressure correction [7]. The variation of the liquid fraction, f_L, in each control volume is evaluated by the modified Lacroix and Voller's method [8] according to the difference in the specific heat between the solid and the liquid phases. The resulting finite difference equations can be written as

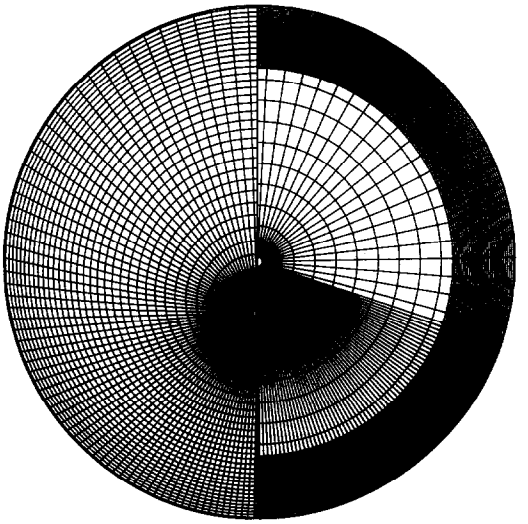

Fig. 2. Grid systems for the low Rayleigh number flow (left) and for high Rayleigh number flow (right)

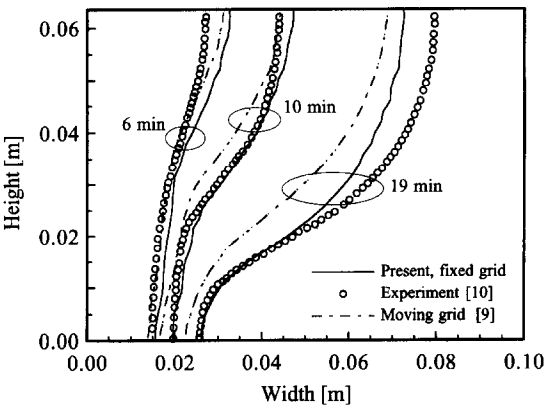

Fig. 3. Variation of the phase interface with time.

$$f_S^{k+1}\left(\frac{\Delta V}{\Delta t}\frac{1}{Ste}\right) = -\sum a_{nb}h_{nb} + \frac{C_L - C_S}{C_L}\frac{\Delta V}{\Delta t}f_S^k h_p^k + \frac{1}{Ste}\frac{\Delta V}{\Delta t}f_S^k \quad (10)$$

$$f_S = 0 \quad \text{if } f_S^{k+1} < 0 \quad (11)$$

$$f_S = 1 \quad \text{if } f_S^{k+1} > 1 \quad (12)$$

where the superscript k denotes each time step, and ΔV, a_{nb} and h_{nb} are control volume, coefficients of the discretized equation and enthalpy of the neighboring control volume, respectively.

The grid dependence of the numerical solution to the unsteady problem such as phase-change heat transfer has been emphasized repeatedly [5, 9]. In this study, the grid dependence has been tested for 36×42, 36×52, 36×62 and 36×72 when the Rayleigh number is relatively small and no distinguishable differences in the results are found when the grid system is 36×52 or larger. However, the 36×72 system is used for more confidence. When the Rayleigh number is large, where the flow at the initial melting stage is major interest, 41×81 is used in order to resolve the complex flow structure and finer grids are allocated near the cylinder bottom wall. Figure 2 shows the grid system for each case. The grid system on the left-hand side is for the small Rayleigh number case and that on the right-hand side is for the large Rayleigh number case.

3. RESULTS AND DISCUSSION

3.1. *Verification of the solution method*

To verify the pertinence and resolvability of the present enthalpy method and the coordinate transformation for predicting complicated thermal and flow phenomena accompanied by the melting process, the results are compared with previous ones by experiments and other numerical methods conducted on the melting processes in two-dimensional rectangular enclosures and horizontal circular cylinders.

Figure 3 compares the present prediction of the phase-interface movement in the case of the Gallium melting in a rectangular enclosure using 42×32 grid system with Gau and Viskanta's [10] experimental results and Viswanath and Jaluria's [9] numerical results. The values of the parameters based on the height as a characteristic length are: $Ra = 6.06 \times 10^5$, $Ste = 0.039$, $Pr = 0.02$ and $Sc = 0.007$. The present phase-interface moves a little faster than Viswanath and Jaluria's, but the overall location and shape of the phase-interface agree fairly well qualitatively and quantitatively with experimental results. The wiggle-shaped phase-interface is a characteristic of the enthalpy method [9], because the interface position is determined from the liquid fraction.

The temperature distribution (left-hand side) and flow pattern (right-hand side) during the melting of the *n*-octadecane in a horizontal circular for $Ra = 3.6 \times 10^5$, $Ste = 0.045$, $Pr = 50$ and $Sc = 0.004$ are plotted in Fig. 4. These are full transient solutions which are obtained without imposing any artificial flow and heat transfer conditions as tried in the previous numerical studies [11, 12] to get multi-solutions. The sequential process that a single-cell appears at the initial melting stage, which is then developed into three-cell structure as the liquid gap is widening and this is merged into a single-cell at the final stage agrees well with the results obtained by the boundary tracking coordinate transformation method [5].

In Fig. 5, the variation of the melting rate with time, which is defined as the ratio of melted mass to total mass, is compared with the pure conduction solution ($Ra = 0$), Ho and Viskanta's experimental results and Ro and Kim's numerical solution. The present result is consistent qualitatively with the well-known fact that the conduction is dominant at the early stage and the natural convection becomes dominant as the melting progresses and agrees well quantitatively with the experimental and other numerical results for the whole melting process.

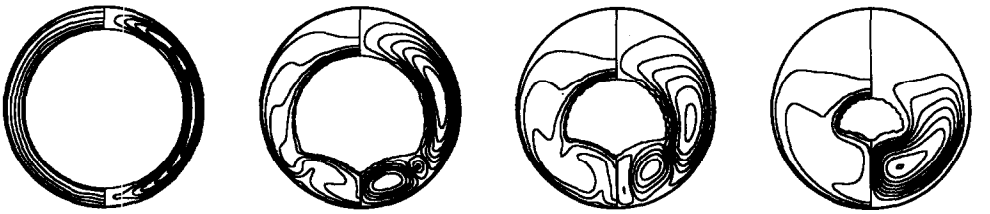

(a) $\tau = 0.018$ (b) $\tau = 0.045$ (c) $\tau = 0.068$ (d) $\tau = 0.086$

Fig. 4. The isotherms (left) and velocity contour (right) at $Ra = 3.6 \times 10^5$, $Ste = 0.045$ and $Sc = 0.004$.

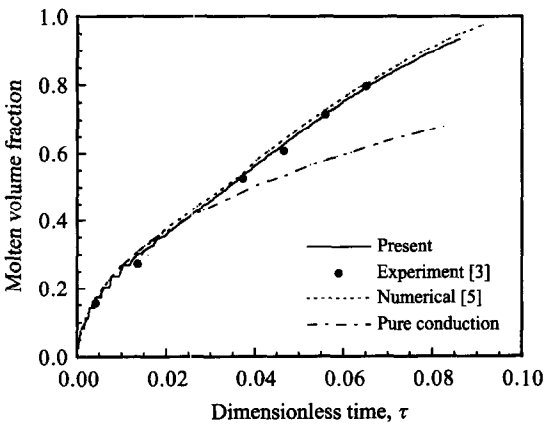

Fig. 5. Variation of the molten volume fraction with time at $Ra = 3.6 \times 10^5$, $Ste = 0.045$ and $Sc = 0.004$.

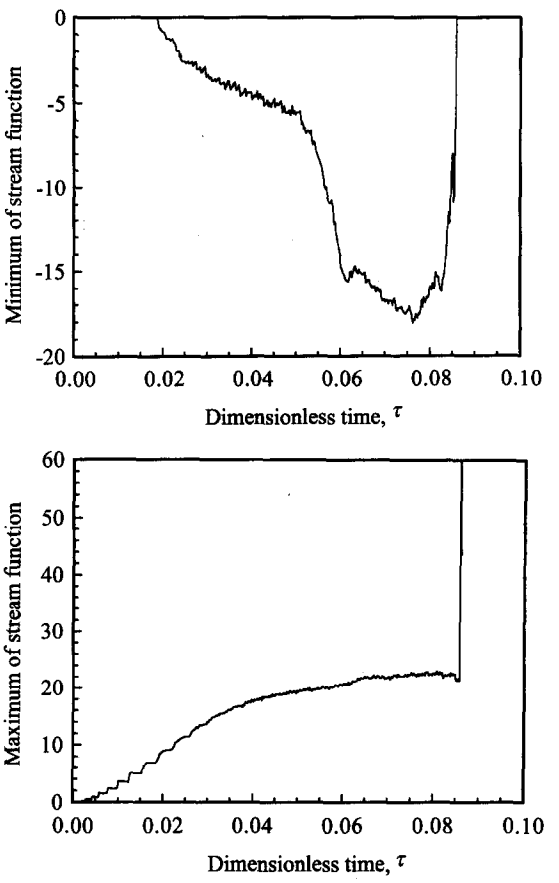

Fig. 6. Variation of maximum and minimum values of the stream function with time.

The heat transfer characteristics in the melting process are usually represented in terms of the Nusselt number variation with time. For example, the effect of natural convection on the total heat transfer is frequently illustrated by comparing the Nusselt number with that corresponding to pure conduction. However, such a comparison cannot give detailed flow information because the Nusselt number variation cannot account for the generation and extinction of the multi-cell structure. In this regard, it is very useful to trace the maximum or minimum of the stream function for identifying the transient flow structure and strength. For example, Fig. 6 shows the trend of the stream function variation corresponding to Fig. 4. From the minimum of the stream function, the time when the multi-cell appears and merges into a single-cell can easily be found at $\tau \approx 0.019$ and 0.086, respectively. The maximum of the stream function visualizes that the multi-cell merges rapidly into a single-cell with a rapid increase in the flow strength. The oscillatory behavior of the stream function variation is due to the unsteady interaction between flow cells as reported by Rieger *et al.* [2].

3.2. *The Rayleigh number effect on the flow pattern*

For a systematic investigation of the Rayleigh number effect on the flow pattern accompanied by the melting, computations are conducted for a relatively wide range of the Rayleigh numbers. The Rayleigh numbers of 1.0×10^4, 3.6×10^5, 1.0×10^6, 5.0×10^6, 1.0×10^7 and 3.0×10^7 are considered. No previous report has been found for $Ra \geqslant 5.0 \times 10^6$.

At the low Rayleigh number ($Ra = 1.0 \times 10^4$) the phase-interface at the early stage is nearly concentric with the cylinder as shown in Fig. 7(a), and only a single-cell exists as a base flow of natural convection. As the melting progresses, the isotherms are changed and the melting at the upper part of the solid is accelerated, as shown in Fig. 7(b), due to natural convection effect, however, no drastic change is observed. As the Rayleigh number increases to 3.6×10^5, the flow changes into a totally different pattern as in Fig. 4 which shows flow transition from the base flow (single-cell) to the three-cell flow at the intermediate stage and finally to the single-cell flow. Such a flow

(a) $\tau = 0.027$ (b) $\tau = 0.158$

Fig. 7. The isotherms (left) and velocity contour (right) at $Ra = 1.0 \times 10^4$, $Ste = 0.045$ and $Sc = 0.004$.

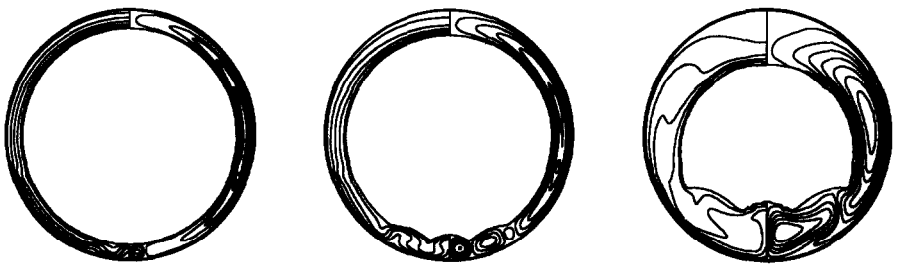

(a) $\tau = 0.009$ (b) $\tau = 0.0135$ (c) $\tau = 0.0315$

Fig. 8. The isotherms (left) and velocity contour (right) at $Ra = 1.0 \times 10^6$, $Ste = 0.045$ and $Sc = 0.004$.

transition at the relatively low Rayleigh number has already been predicted by the previous studies [5, 11].

When the Rayleigh number becomes relatively high ($Ra = 1.0 \times 10^6$), the flow undergoes another change as shown in Fig. 8. At the early stage, transition from the two-cell to the four-cell structure is observed and then the four-cell merges into the two-cell as time elapses. At a first look, this flow behavior seems similar to Ro and Kim's secondary bifurcating solution [5] which is obtained at $Ra = 1.2 \times 10^6$. However, the present solution is not an artificial one such as the secondary bifurcating solution, but a full transient solution. In addition, while their secondary bifurcating solution shows a transition directly from the base flow to the four-cell flow, the present solution reveals a gradual transition of two-cell, four-cell and two-cell in due sequence. This difference suggests that the appearance of the four-cell structure at the high Rayleigh number should be explained by an analysis associated with natural convection, not by the artificial method. This fact can be confirmed by the computations at the higher Rayleigh numbers.

Figures 9–11 illustrate the flow behavior at the higher Rayleigh numbers of 5.0×10^6, 1.0×10^7 and 3.0×10^7, respectively, which have not been conducted before. To clearly see the details of the flow and heat transfer characteristics, presented are locally magnified plots at the upper and lower parts of the cylinder. The multi-cell structure in the liquid region near the bottom of the cylinder appears earlier and the cell number increases as the Rayleigh number increases. At a given Rayleigh number, the flow is branched off upto a certain number of cells as time passes by, and then only the flow strength increases afterwards.

Based on the above observation, firstly, it is confirmed that the contradictory results of the two- or three-cell structure at the same condition as indicated earlier in the introduction are both possible. The Rayleigh numbers considered in previous studies fall in the intermediate range where both of the base flow (single-cell) and the multi-cell structure appear and they correspond to the neutrally stable conditions where the thermal buoyancy and viscous forces are in balance. Thus, the possibility of a transition from one flow pattern to another by a numerical disturbance always exists. The numerical disturbance may be originated from the differences in the numerical method, initial condition, relaxation factor and algorithm. Secondly, the present results also ensure the existence of the multi-cell structure (more than four cells) even for the high Prandtl number fluids. Many studies have focused on the multi-solution of the natural convection between concentric cylinders, however, these studies are limited to the small Prandtl numbers where the hydrodynamic instability is dominant. Actually, Cheddadi *et al.* [12] visualized the two-cell structure by imposing an initial condition given by a specific functional type, and Kim and Ro [13] found the three-cell structure by a rather improved method, however, no other studies could predict the existence of the four-cell structure by any means. From this point of view, the present approach, which can predict the multi-cell structure by the general and reproducible method, can be applied to the natural convection

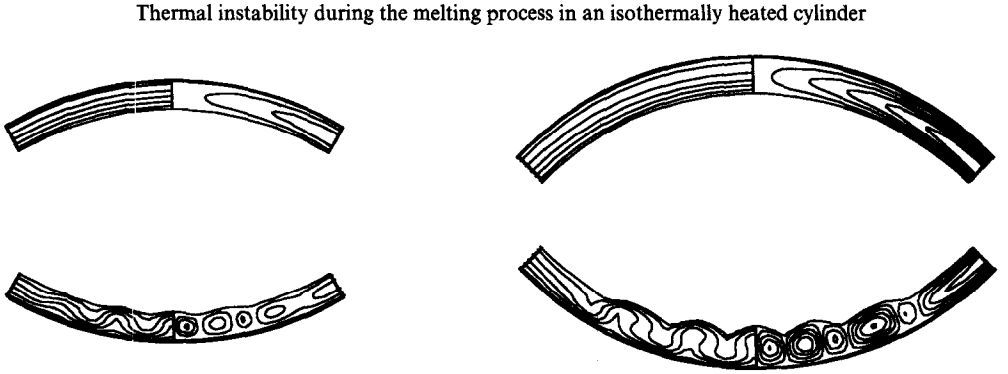

(a) $\tau = 0.00315$ (b) $\tau = 0.045$

Fig. 9. The isotherms (left) and velocity contour (right) at $Ra = 5.0 \times 10^6$, $Ste = 0.045$ and $Sc = 0.004$.

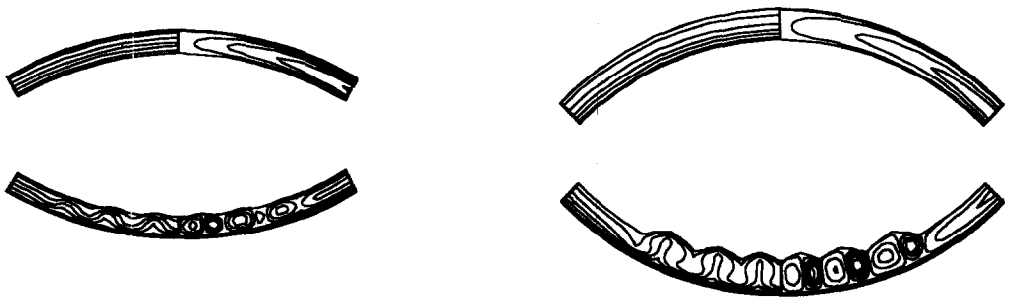

(a) $\tau = 0.0018$ (b) $\tau = 0.00338$

Fig. 10. The isotherms (left) and velocity contour (right) at $Ra = 1.0 \times 10^7$, $Ste = 0.045$ and $Sc = 0.004$.

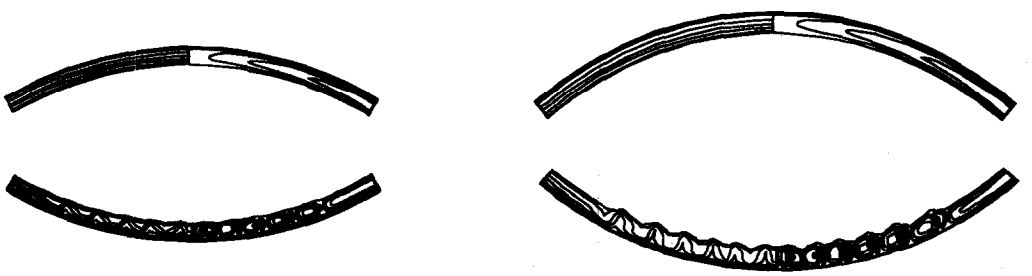

(a) $\tau = 0.0009$ (b) $\tau = 0.00135$

Fig. 11. The isotherms (left) and velocity contour (right) at $Ra = 3.0 \times 10^7$, $Ste = 0.045$ and $Sc = 0.004$.

problem between the concentric cylinders. Finally, a regularity in the relation between cell size and liquid gap is found in response to the Rayleigh number variation. This fact suggests that the origin of the multi-cell structure can be analyzed by the stability theory for the thermally unstable liquid layer in a fixed region.

3.3. *Thermal instability at the high Rayleigh number*

At the high Rayleigh number the multi-cell flow at the initial melting stage creates nearly regular wave-shaped phase-interface by its alternate rotating motion in the clockwise and counter-clockwise directions. This phenomenon is very similar to the Benard convection due to the thermal instability because the phase-interface and the cylinder bottom wall can be approximated as two flat plates as far as the liquid gap between these two surfaces is narrow enough. Thus, the linear stability theory can be applicable. According to the linear stability theory for the flow which has unstable temperature gradient between two flat plates [14], the effective Rayleigh number where the natural convection starts to occur is a function of the wave number. It is known that the critical Rayleigh number, which is the minimum of the effective Rayleigh number, is 1707.762 at the wave number of 3.117.

Table 3. Effective Rayleigh number and wave number at the on-set of convection

Cases (Ra)	Ra_{eff}	a
1.0×10^6	2380.9	2.5538
5.0×10^6	2035.7	2.8544
1.0×10^7	1820.5	2.4975
3.0×10^7	1803.8	3.8680

Here, the characteristic length of the effective Rayleigh number is the liquid layer length and the wave number can be calculated from the wavelength defined as the distance between the cells which have the same flow direction.

The liquid gap and wavelength at the point of the emergence of the multi-cell are obtained for four different Rayleigh numbers of $Ra \geqslant 1.0\times10^6$. Because the phase-interface is wavy, the average values are taken for the liquid gap over the region where the multi-cell exists, and the wavelengths are measured from the temperature distribution because it shows more regular pattern than the flow cell. The results for the liquid gap, the effective Rayleigh number converted from the Rayleigh number and the wave number evaluated from wavelength are summarized in Table 3. They are also plotted in Fig. 12 with the neutral stability curve of the Benard convection. Even though the uncertainties may be present associated with the cylinder curvature, on-set of the multi-cell and irregularity of the phase-interface shape, the present results are in excellent agreement with the linear stability theory. This fact implies that the generation mechanism of the multi-cell structure is essentially the same as that of the Benard convection. It is also obvious that the cylinder curvature and the irregularity of the phase-interface shape do not practically affect the flow induced by the thermal instability though they may cause non-uniformity in the cell shape and size. The effective Rayleigh number approaches the neutral stability curve as the Rayleigh number increases because the liquid gap is getting narrower so that the natural convection occurs at the more similar condition to that between the flat plates.

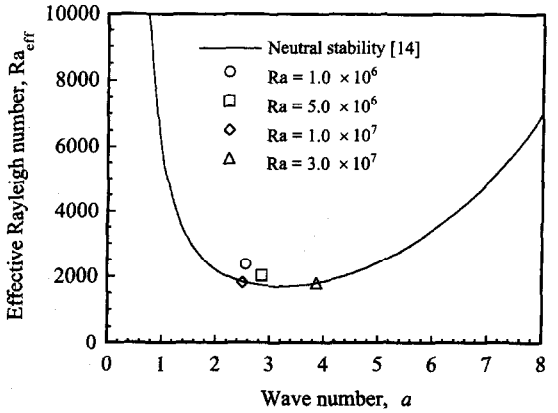

Fig. 12. Comparison of the present effective Rayleigh number with that of the linear stability theory.

From the above observation, the emergence of the multi-cell structure in the melting process in the horizontal circular cylinder can be reanalysed from the linear stability theory point of view. For example, in the case of $Ra = 1.0\times10^4$, the liquid gap is about $0.555R_w$ to reach the critical Rayleigh number, however, the linear temperature distribution which is necessary to bring about the Benard convection is not formed because the base flow is fully developed before reaching the critical condition. On the other hand, in the case of $Ra = 5.0\times10^6$ where the critical liquid gap is about $0.07R_w$, the condition for the on-set of the multi-cell structure is fully satisfied because the base flow is so weak that the linear temperature profile is sustained (see the temperature distribution against the base flow in Fig. 9). These two Rayleigh numbers fall in each Rayleigh number range which shows clear distinction in the flow structure. However, in the case of $Ra = 3.6\times10^5$ and 1.0×10^6, which have been considered in the previous studies, the critical liquid gaps are $0.168R_w$ and $0.120R_w$, and the Benard convection has already been affected at the beginning by the base flow under development. Therefore, the previous contradictory results seem to be brought about due to the different numerical methods which might include several types of uncertainties. Thus, it is no wonder that Ro and Kim's [5] artificial change of the initial conditions showed the possibility of both contradictory results at such a neutrally stable state. Their full transient solution of the bifurcation solutions cannot be guaranteed to be reproducible if another numerical method is used. The present result for $Ra = 1.0\times10^6$, as discussed earlier, supports this remark.

In view of the results so far achieved, the qualitative variation of the flow pattern by the thermal instability can be summarized as follows: at the low Rayleigh number, the base flow is fully developed and prevails in the whole flow region before the condition for the on-set of the Benard convection is reached; at the intermediate Rayleigh number, the on-set of the Benard convection is closely related to the strength of the base flow and a delicate interaction between the two flows determines the flow pattern afterwards; and at the high Rayleigh number, the Benard convection is not practically affected by the base flow and develops with a certain level of regularity.

4. CONCLUSIONS

The multi-cell structure and the thermal instability at the early stage of the melting process in the horizontal cylinder have numerically been analyzed for a relatively wide range of the Rayleigh numbers including the intermediate Rayleigh numbers at which the previous studies have shown the contradictory results. Several important observations are noted and summarized below.

(1) The enthalpy method is an efficient solution method, particularly when the grid generation is not easy by the boundary tracking method due to the irregular phase-interface shape.

(2) At the low Rayleigh number, the flow in the liquid gap is in the stable state because the base flow has already been fully developed before the on-set of the Benard convection.

(3) At the intermediate Raleigh number, the thermal buoyancy and the viscous forces are balanced in a neutrally stable state. Thus, the flow is prone to transit to different patterns by infinitesimal experimental or numerical disturbances.

(4) At the high Rayleigh number, the Benard convection shows an orderly behavior without being affected by the base flow. The effective Rayleigh number which is corresponding to the wavelength defined as the distance between the adjacent cells which have the same flow direction at each Rayleigh number collapses on the neutral stability curve obtained by the linear stability theory.

REFERENCES

1. Saitoh, T. and Hirose, K., High Rayleigh number solutions to problems of latent heat thermal energy storage in a horizontal cylinder capsule. *ASME Journal of Heat Transfer*, 1982, **104,** 545–553.
2. Rieger, H., Projahn, U., Bareiss, M. and Beer, H., Heat transfer during melting inside a horizontal tube. *ASME Journal of Heat Transfer*, 1983, **105,** 226–234.
3. Ho, C. J. and Viskanta, R., Heat transfer during inward melting in a horizontal tube. *International Journal of Heat and Mass Transfer*, 1984, **27,** 705–716.
4. Yoo, H. S. and Ro, S. T., Numerical analysis of the phase change processes by coordinate transformations. *Transactions of KSME*, 1986, **10,** 585–592.
5. Ro, S. T. and Kim, C.-J., Bifurcation phenomenon during the fixed-solid-mode melting inside a horizontal cylinder. *International Journal of Heat and Mass Transfer*, 1994, **37,** 1101–1109.
6. Fant, D. B., Prusa, J. and Rothmayer, A. P., Unsteady multicellular natural convection in a narrow horizontal cylindrical annulus. *ASME Journal of Heat Transfer*, 1990, **112,** 379–387.
7. Patankar, S. V., *Numerical Heat Transfer and Fluid Flow*. Hemisphere, New York, 1980.
8. Lacroix, M. and Voller, V. R., Finite difference solutions of solidification phase change problems: transformed vs fixed grids. *Numerical Heat Transfer, Part B*, 1990, **17,** 25–41.
9. Viswanath, R. and Jaluria, Y., A comparison of different solution methodologies for melting and solidification problems in enclosures. *Numerical Heat Transfer, Part B*, 1993, **24,** 77–105.
10. Gau, C. and Viskanta, R., Melting and solidification of a pure metal on a vertical wall. *ASME Journal of Heat Transfer*, 1986, **108,** 174–181.
11. Park, C. E. and Chang, K.-S., Bifurcating solutions of inward melting in a horizontal tube. *Transport Phenomena in Heat and Mass Transfer*, ed. J. A. Reizes. Elsevier, Amsterdam, 1992, pp. 704–714.
12. Cheddadi, A., Caltagirone, J. P., Mojtabi, A. and Vafai, K., Free two-dimensional convective bifurcation in a horizontal annulus. *ASME Journal of Heat Transfer*, 1992, **114,** 99–106.
13. Kim, C.-J. and Ro, S. T., Numerical investigation on bifurcative natural convection in an air-filled horizontal annulus. *Proceedings of the Tenth International Heat Transfer Conference*, Vol. 7. Taylor & Francis, 1994, pp. 85–90.
14. Chandrasekhar, S., *Hydrodynamic and Hydro-Magnetic Stability*. Oxford University Press, 1961.